Measurements of Thorium and Uranium daughters in Radioenvironmental Samples Using $\gamma\gamma$-Coincidence Spectrometry☆

Andrew Tillett[a], Larry Benninger[b], John Dermigny[a,c], Christian Iliadis[a,c,*]

[a] *Department of Physics and Astronomy, The University of North Carolina at Chapel Hill, Chapel Hill, North Carolina 27599, USA*
[b] *Department of Geological Sciences, The University of North Carolina at Chapel Hill, Chapel Hill, North Carolina 27599, USA*
[c] *Triangle Universities Nuclear Laboratory (TUNL), Durham, North Carolina 27708, USA*

Abstract

We present the performance of a $\gamma\gamma$-coincidence spectrometer for measuring the activities of thorium and uranium daughters in environmental samples. The spectrometer consists of two NaI(Tl) detectors facing each other inside a low-background passive shield. We present coincidence gating schemes for achieving the best signal-to-noise ratios, coincidence detection efficiencies, background levels, and minimum detectable activities. The spectrometer is simulated using Geant4 to correct sample efficiencies for self-absorption effects. The device is used to measure thorium and uranium daughter activities in Brazil nuts, potting mix, and magazine paper. Our results for Brazil nuts agree with some, but not all, previous measurements. Thorium or uranium daughter activities have previously not been reported for commercial potting mix. For magazine paper, our measured activities are lower than most previously determined values.

Keywords: `elsarticle.cls`, LaTeX, Elsevier, template

2010 MSC: 00-01, 99-00

1. Introduction

Understanding the effect of naturally occuring radionuclides, such as the uranium and thorium series, on humans requires a detailed understanding of their behavior in the environment. These nuclides are continually being redistributed by various natural mechanisms and can thus serve as tracers of the various biological, meteorological, or geophysical processes. Studies of environmental radioactivity require the availability of sensitive techniques capable of measuring concentrations at very low levels in small samples. In addition, the investigation of complex mixtures of naturally occuring radionuclides requires highly selective measurement techniques. Because of their supreme energy resolution, many investigators have used for this purpose high-purity Germanium (HPGe) detectors with complex passive shields, sometimes located in deep

*Corresponding author
Email address: `iliadis@unc.edu` (Christian Iliadis)

underground laboratories. Spectrometers based on NaI(Tl) crystals represent an interesting and affordable[1] alternative, especially if they involve $\gamma\gamma$-coincidence spectrometry [1, 2, 3, 4, 5, 6, 7, 8]. The advantages are significant, since (i) samples of small sizes can be assayed, (ii) the identification of the radionuclides is virtually unambiguous, (iii) the counting times are reasonable, and (iv) minimum sample preparation is involved, thereby greatly reducing the risk of accidental contamination.

Recently, such an instrument consisting of two NaI(Tl) detectors has been commissioned at The University of North Carolina at Chapel Hill. The performance of the instrument for detecting positron-emitting radionuclides, including the measurement of the cosmogenic ^{26}Al activity in a small (18 g) meteorite fragment, has been described in Ref. [9]. Here, we discuss the performance of the spectrometer for detecting thorium and uranium daughters in samples of Brazil nuts, potting mix, and magazine paper.

The $\gamma\gamma$-coincidence spectrometer is described in Section 2. Procedures and detection schemes are presented in Section 3. Measurements and results are discussed in Section 4. Conclusions are given in Section 5.

2. Equipment

The spectrometer is shown in Figure 1. It consisted of two NaI(Tl) detectors, which faced each other at a distance of 38.1 mm along their symmetry axis. Each detector contained a crystal with a diameter of 152.4 mm and length of 101.6 mm, inside an aluminum housing with a wall thickness of 0.81 mm. The crystals were coupled to photomultiplier tubes of 127.0-mm diameter via low-background optical quartz windows. The only spectrometer part selected for low-background radiation was the optical window.

The detectors were surrounded by several layers of different metals. The innermost layer consisted of 0.64-cm thick copper, surrounded by 10.2-cm thick lead. The outermost layer was made of 1.0-cm thick aluminum and provided support for the shielding above the detectors. The top shield consisted of a low-background steel plate of 2.0-cm thickness, which supported a 10.2-cm-thick layer of lead bricks and another 2.0-cm-thick steel plate. A 10.2-cm-diameter hole at the center of the top shield provided convenient access to the sample (shown in green in Figure 1) located between the two detectors.

A lead plate of 2.54-cm thickness was located between the detector front faces to reduce background coincidence events caused by γ-rays that Compton scatter between the detectors. Background radiation was reduced by factors of $2 - 4$ by this shield, depending on the coincidence gate used. This lead plate had a central hole of 3.8-cm diameter, with tapered edges to reduce the absorption of γ-rays originating from the sample.

[1] The total cost of our spectrometer was about $50,000, including the two detectors, passive shielding, electronics, computer, and the machining of parts. It is thus much less expensive than a HPGe-based setup, which in addition requires the use of liquid nitrogen.

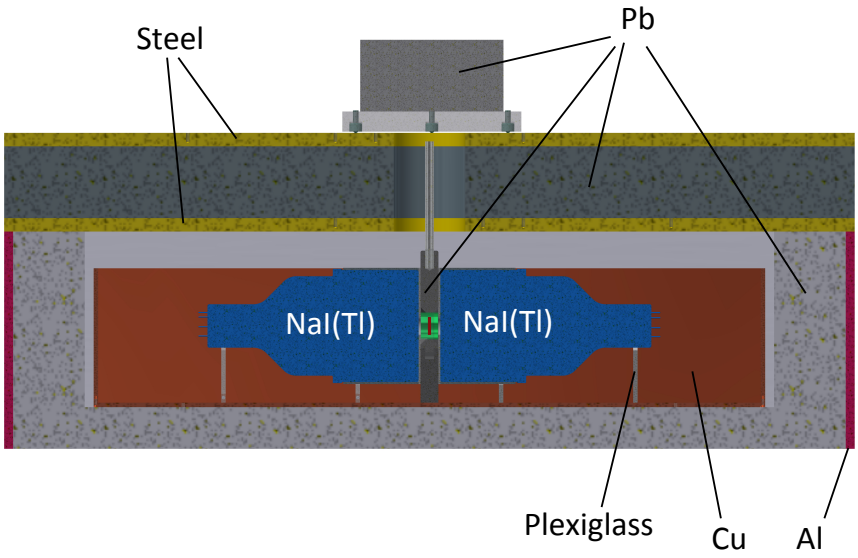

Figure 1: (Colour online) Cross-sectional views of the $\gamma\gamma$-coincidence spectrometer, showing the geometry and different layers of materials. Part of the lead shield, located between the two detectors, was removable and contained the sample holder (shown in green). Each detector contained a crystal with a diameter of 152.4 mm and length of 101.6 mm. See also Figure 2 in Ref. [9].

The output signal from each detector was split into two branches without pre-amplification. The first signal was processed by a spectroscopy amplifier and was subsequently fed into a 4096-channel VME amplitude-to-digital converter (ADC). The second signal was processed by a fast timing filter amplifier (TFA), and was then fed into a constant-fraction discriminator (CFD). The logic output signal provided the gate for the ADC and the start and stop signals for the time-to-amplitude converters (TAC). The output of the TAC was also fed into the ADC. The data were stored in list mode for subsequent offline analysis, where each event consists of the energy and timing information for both detectors. All timing and energy coincidence gating was performed using the data acquisition system JAM [10].

Several cyclindrical sample holders were fabricated from aluminum. The outer diameter and width were 3.70 cm and 2.70 cm, respectively. The average wall thickness was $\approx$ 1 mm, resulting in an inner cavity volume of 24.05 cm^3. The sample inside the holder was hermetically sealed using a Viton O-ring.

3. Procedures

3.1. Reference Materials and Environmental Samples

For the measurement of uranium and thorium daughters in environmental samples via γ-ray spectrometry, standards are produced from natural materials for which secular equilibrium can be assumed. For

thorium, we used the CRM 107-A reference material, which is certified by the New Brunswick Laboratory[2]. This material was prepared by diluting monazite (rare-earth and thorium phosphate) sand with silica (99.9% SiO_2, essentially free of radioactivity). New Brunswick Laboratory used spectrophotometry to determine a resulting thorium content of $0.1028 \pm 0.0002\%$ by weight. The total mass of our reference sample was 13.263 g, resulting in a ^{232}Th activity of 55.4 ± 0.1 Bq. The CRM 107-A sample includes a minor uranium component of 0.00408% by weight, as calculated from the uranium content of the parent monazite sand.

Our uranium standard was reference uranium ore BL-4a, obtained from the Canada Centre for Mineral and Energy Technology[3]. The BL-4a sample consisted of pitchblende (massive uraninite) in feldspar and hematite. The certified uranium content was $0.1248 \pm 0.0007\%$ by weight, corresponding to 15.41 Bq ^{238}U per gram of BL-4a. Also certified are the daughters ^{226}Ra and ^{210}Pb, which are in secular equilibrium with ^{238}U within stated uncertainties (<4%, at 95% confidence). The total mass of our reference sample was 22.048 g, resulting in a ^{226}Ra activity of 341 ± 2 Bq.

The three environmental samples, i.e., Brazil nuts, potting mix, and magazine paper, had masses of 17.980 g, 7.226 g, and 24.231 g, respectively. The Brazil nuts were purchased from a local grocery store, and were grown in Bolivia and Peru. The potting mix was purchased from Miracle-Gro®. These samples were dried in an oven for approximately forty-eight hours. Before they were sealed in the aluminum sample holders, the Brazil nuts (edible portion only) were ground into a coarse powder and the potting mix was sifted to remove large pieces of debris. The paper was collected from a sports magazine published in the United States. Circular shapes were cut from the magazine pages and were densely packed into the sample holder.

The three samples were stored for approximately one month. In the thorium series, ^{224}Ra has a half-life of 3.6 d, and in the uranium series, ^{222}Rn has a half-life of 3.8 d. A waiting period of one month corresponds to approximately ten half-lives for these radioisotopes, and thus ensures that the radioistopes whose decay we were planning to measure (^{208}Tl and ^{214}Bi; see below) are in secular equilibrium with longer-lived radioisotopes further up the decay series.

For estimating the γ-radiation background, we filled a sample holder with distilled water. This sample was periodically measured to account for potential time variations in the radiation background. Also, before and after each sample run, the energy calibrations of both NaI(Tl) detectors were checked using ^{22}Na and ^{60}Co calibration sources [9].

3.2. Coincidence Gating Schemes

Figure 2 shows two-dimensional histograms of the energy deposited in detector 2 versus the energy deposited in detector 1. The results displayed in the top and bottom panels were measured using the

[2]https://science.energy.gov/nbl.

[3]http://www.nrcan.gc.ca/mining-materials/certified-reference-materials/7827.

thorium (top) and uranium (bottom) reference material, respectively. Both histograms display groups of different coincidence events, depending on which and how many of the γ-rays simultaneously emitted by the sample are detected in the spectrometer. The pairs of numbers correspond to energies (in keV) detected in each counter, while the red rectangles show coincidence gates used to generate gated one-dimensional pulse-height spectra (see below). Notice the symmetry around the diagonal equal-energy line.

For thorium, the best coincidence gate to use is based on the full-energy deposition of 2614 keV in one detector, indicated by the red rectangles in the top panel of Figure 2. This γ-ray is produced in the β-decay of ^{208}Tl, and corresponds to the deexcitation of the first excited state to the ground state in the daughter ^{208}Pb. The black arrows indicate the γ-rays that are coincident with the 2614 keV photon. The highest intensity regions inside the two red gates correspond to 2614-keV photons depositing energy in one detector and the coincident 583 keV or 511 keV photons depositing energy in the other detector (labeled by "2614, 583" or "2614, 511", respectively). The 511-keV γ-ray originates from the transition of the fourth excited state to the second excited state in ^{208}Pb, and incidentally has the same energy as electron-positron annihilation photons. Most of the other coincidence events, at lower energies, originate from the radioactive decays of ^{208}Tl, ^{228}Ac, and ^{212}Bi, which are all part of the ^{232}Th decay series. However, notice the coincidence events (labeled "U") that are slightly offset from the 583-keV vertical and horizontal bands. They originate from the ^{238}U decay series and reveal a small uranium contamination in the thorium reference material.

For uranium, a convenient coincidence gate is based on the full-energy deposition of 609 keV in one detector (red rectangles in bottom panel of Figure 2). This γ-ray is produced in the β-decay of ^{214}Bi, and corresponds to the deexcitation of the first excited state to the ground state in the daughter ^{214}Po. The highest intensity regions inside the two red gates correspond to 609-keV photons depositing energy in one detector and the coincident 1120 keV or 1238 keV photons depositing energy in the other detector (labeled by "609, 1120" or "609, 1238", respectively). Notice the group of coincidence events (labeled "Th") near the high-energy end of the red gates that are slightly offset from the 609-keV vertical and horizontal bands. They are caused by (2614, 583) coincidence events from a small thorium contamination in the uranium reference material.

The events inside the two-dimensional gates were projected onto the horizontal (energy of detector 1) and vertical (energy of detector 2) axes and the resulting pulse-height spectra were summed to produce a composite one-dimensional coincidence histogram for count rate estimates. The results are shown in Figure 3 for the thorium reference sample (top panel) and the uranium reference sample (bottom panel). For the activity of thorium (or progeny), we analyzed the total number of counts in the energy region from 444 keV to 669 keV (indicated by the two vertical dashed lines in the top panel). This energy region is dominated by ^{208}Tl-decay photons of 511 keV and 583 keV, which are in coincidence with 2614-keV photons. For the activity of uranium (or progeny), we analyzed the total number of counts in the energy region from 1024 keV to 1324 keV (indicated by the two vertical dashed lines in the bottom panel). This energy region

is dominated by ^{214}Bi-decay photons of 1120 keV and 1238 keV, which are in coincidence with 609-keV photons.

If a sample containing both thorium and uranium (or their progenies) is measured, the thorium activity should be determined first since none of the coincident photons from ^{214}Bi decay are expected to contaminate the 2614-keV energy gate. Once the thorium activity has been determined, the likely contamination of the 609-keV gate by coincident photons from ^{208}Tl decay can be estimated with the help of computer simulations (see Section 3.3).

3.3. Coincidence Detection Efficiencies and Simulations

To determine the activities of extended (volume) sources from measured coincidence intensities in a given energy region of interest, we needed to correct the experimental detection efficiencies that are associated with a particular coincidence gate. We proceeded in two steps. First, we determined experimental coincidence efficiencies using the thorium and uranium reference samples for which the absolute activities are precisely known (Section 3.1). Second, we performed computer simulations to account for differences of the self-absorption in the various environmental samples.

Experimental efficiencies were determined for the thorium and uranium decay series using coincident photons from the decay of ^{208}Tl and ^{214}Bi, respectively. The coincidence gates (2614 keV and 609 keV, respectively) and energy regions ($444 - 669$ keV and $1024 - 1324$ keV, respectively) are shown in Figures 2 and 3. Results are listed in Table 1. For thorium and uranium, the coincidence efficiencies were $0.629 \pm 0.003\%$ and $0.794 \pm 0.005\%$, respectively. The former value implicitly includes the 36% branching of the ^{212}Bi decay to ^{208}Tl. Our efficiencies are a factor of two lower than the results of Ref. [11], who employed a larger coincidence spectrometer.

Monte Carlo simulations of detection efficiencies were performed with the Geant4 toolkit, version 9.6 [13]. All components of the setup, including the detectors, the lead plate between them, the passive shielding (copper, steel, lead), and the extended sample geometry, were incorporated into the Geant4 model. The thorium and uranium standard samples were simulated with chemical compositions based on the information provided by the suppliers (see Section 3.1). The thorium reference sample consisted mainly of cerium phosphate, lanthanum phosphate, neodymium phosphate, and thorium phosphate, while the uranium reference sample consisted mainly of silicon dioxide, aluminum oxide, and iron oxide. The simulations assumed volume-source geometries and densities close to those of the actual reference samples.

In the simulations, it was assumed that only decays of the radioisotope of interest occured. The γ-ray decays of the various radioisotopes belonging to the thorium and uranium decay series are built into Geant4, and are based on the Evaluated Nuclear Structure Data Files (ENSDF) managed by Brookhaven National Laboratory. For the thorium reference sample, we simulated the decay of ^{212}Bi in place of ^{208}Tl, the radioisotope of interest, to take into account the branching ratio of ^{212}Bi as it decays to either ^{208}Tl (36%) or

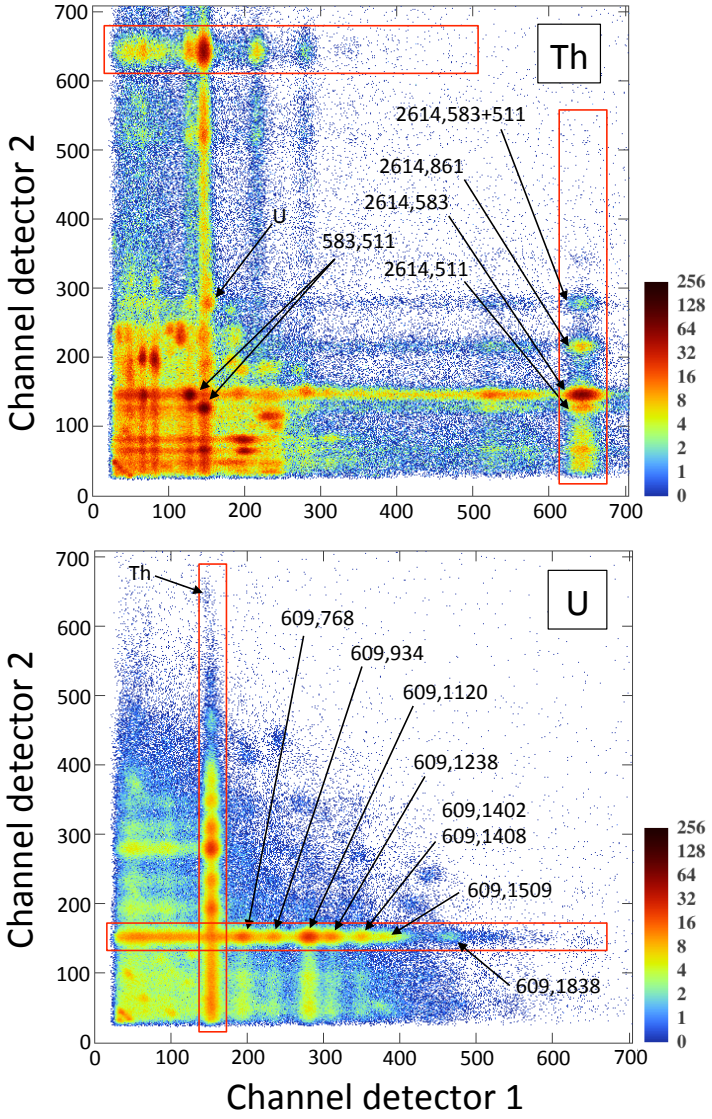

Figure 2: (Colour online) Measured two-dimensional histogram of energy deposited in detector 2 versus energy deposited in detector 1. The axes show channels, not energy. The red rectangles represent coincidence gates that are most useful for the detection of a given material. The pairs of numbers correspond to energies (in keV) detected in both counters. (Top) Thorium reference material. The red rectangles are based on the detection of 2614 keV photons from ^{208}Tl decay in one detector. The most intense coincidence group corresponds to the detection of 2614 keV photons in one detector and 583 keV photons in the other detector. Notice the small uranium contamination labeled "U". (b) Uranium reference material. The red rectangles are based on the detection of 609 keV photons from ^{214}Bi decay in one detector. The most intense coincidence group corresponds to the detection of 609 keV photons in one detector and 1120 keV photons in the other detector. Notice the small thorium contamination labeled "Th".

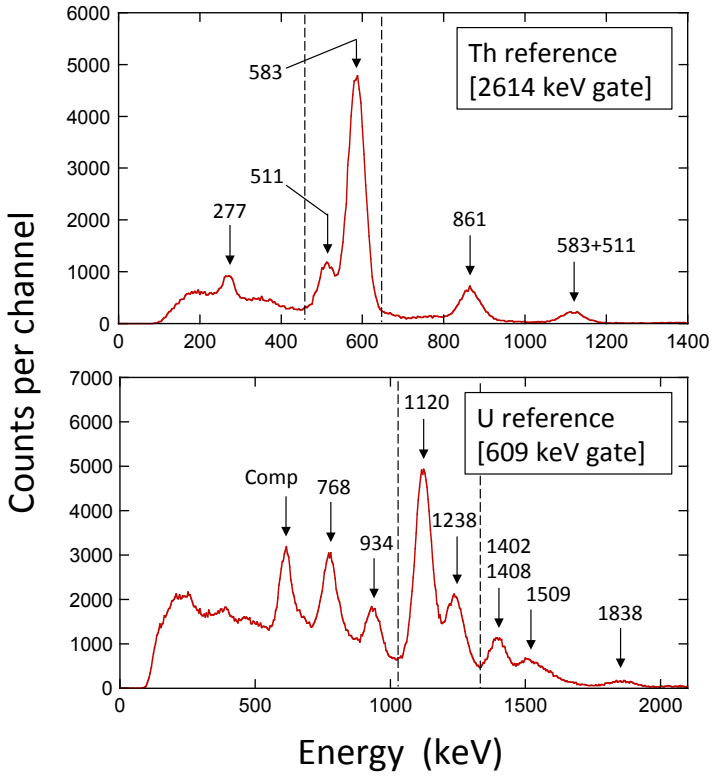

Figure 3: (Colour online) Measured one-dimensional histograms of events located inside the red coincidence gates shown in Figure 2. In the present work, we analyzed the total number of counts in the energy region between the two vertical dashed lines to estimate the activity of the sample. (Top) Thorium reference material. A 2614 keV γ-ray (from ^{208}Tl decay) is detected in either of the two counters, while coincident photons of various energies (values in keV) are detected in the other counter. The peak at 1094 keV originates from the simultaneous detection of the coincident 583 keV and 511 keV photons in one counter ("583+511"). (Bottom) Uranium reference material. A 609 keV γ-ray (from ^{214}Bi decay) is detected in either of the two counters, while coincident photons of various energies (values given in keV) are detected in the other counter. The peak labeled "Comp" originates from Compton-scattered ^{214}Bi-decay photons that end up in the 609 keV coincidence gate (red rectangles in bottom panel of Figure 3).

^{212}Po (64%). For the uranium reference sample, the decay of ^{214}Bi was simulated. The simulated efficiency implicitly includes the γ-ray branching ratios. Because the simulation did not account for energy resolution, we convolved the simulated spectra with an energy dependent Gaussian function before determining the efficiencies. The Gaussian function had the same full width at half maximum as the measured peak for the same γ-ray energy. We defined the simulated detection efficiency in the same manner as the experimental efficiency, i.e., as the ratio of the total intensity in the region of interest and the total number of decaying nuclei.

Simulations were performed for twenty-four million events for each sample, assuming hypothetical reference materials of thorium (i.e., without uranium) and uranium (i.e., without thorium). Simulated coincidence spectra are shown in Figure 4 and can be compared to the corresponding measured spectra shown in Figure 3. It can be seen that the simulations reproduce all essential features of the experimental spectra. The simulated coincidence efficiencies are listed in Table 1. The quoted errors represent statistical uncertainties based on the number of counts in the coincidence regions of interest in the simulated spectra. The uncertainties are inversely proportional to the total number of simulated events. Measured and simulated coincidence efficiencies for the thorium and uranium reference samples agree within ≈3%. Notice that no arbitrary scaling of the simulation results was performed.

The simulations were repeated for the environmental samples and the results are listed in Table 1. The coincidence efficiencies are also displayed in Figure 5 versus the sample density. The black and red data points correspond to the simulated and measured efficiencies, respectively. The simulated efficiencies for Brazil nuts (ρ = 0.747 g/cm^3) and magazine paper (ρ = 1.007 g/cm^3) are close to the measured values for the thorium and uranium reference materials. Because of the much lower sample density, the simulated efficiencies for the potting mix (ρ = 0.300 g/cm^3) are higher by ≈ 10% compared to the reference material values. Our results support the finding of Paradis et al. [14] that in the γ-ray energy range above a few hundred keV, the self-absorption depends mainly on the sample density. At lower γ-ray energies, we expect that the sample composition would also impact the coincidence efficiencies.

3.4. Background Radiation

Coincidence background spectra, obtained using distilled water in the sample holder, are shown in Figure 6. The measurement time was 3.0 d. The top and the bottom panels correspond to the same coincidence gates shown in the top and bottom panels of Figures 2 and 3. The regions of interest (444 − 669 keV and 1024 − 1324 keV for the 2614 keV and 609 keV gates, respectively) are indicated by vertical dashed lines. The coincidence background count rates (in counts per minute) are listed in the fourth column of Table 2 and can be compared to the singles count rates listed in the third column. The reduction in background amounts to about three orders of magnitude. Our coincidence background is lower than that of Ref. [11], by a factor of ≈ 1.7, presumably because larger detectors were used in the previous work.

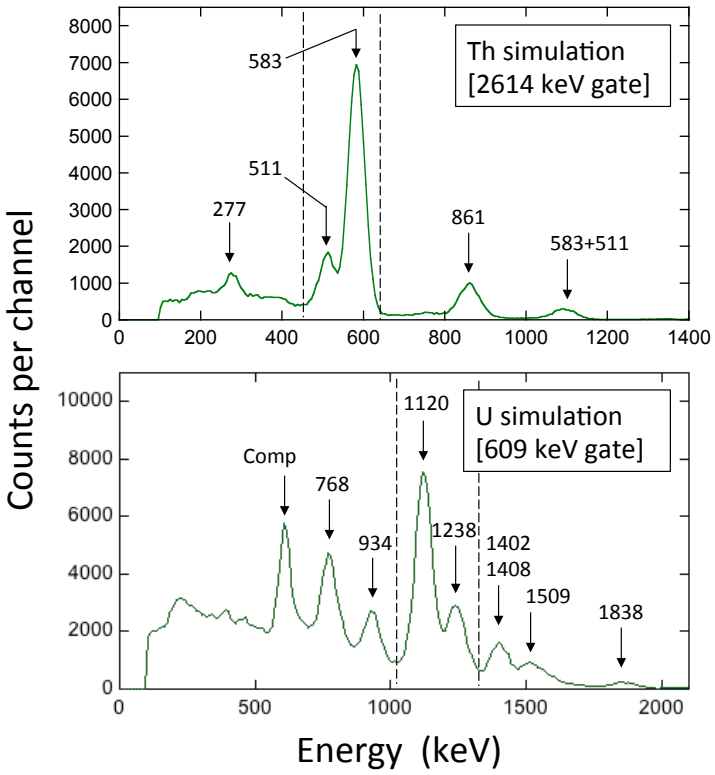

Figure 4: (Colour online) Geant4 simulations of events located inside the red coincidence gates shown in Figure 2. These spectra can be compared to the measured ones shown in Figure 3. The region between the two dashed lines marks the energy region of interest. (Top) Thorium material, i.e., without any uranium contamination. (Bottom) Uranium material, i.e., without any thorium contamination.

Table 1: Present experimental (labeled "exp") and simulated coincidence efficiencies, η, for various samples. The efficiency is defined as the total intensity in a given region of interest divided by the total number of decaying nuclei during the counting or simulation time period. The values are normalized to unity, e.g., 0.0065 ± 0.0005 corresponds to $0.65 \pm 0.05\%$.

Sample[a]	Density (g/cm^3)	η_{2614}[b]	η_{609}[b]
Th standard	0.551	0.00629 ± 0.00003[c](exp)	
		0.0065 ± 0.0005	
U standard	0.917		0.00794 ± 0.00005[d](exp)
			0.0082 ± 0.0005
Brazil nuts	0.747	0.0063 ± 0.0003	0.0083 ± 0.0005
Potting mix	0.300	0.0068 ± 0.0004	0.0091 ± 0.0006
Magazine paper	1.01	0.0062 ± 0.0003	0.0080 ± 0.0005

[a] See text.

[b] The regions of interest were: $444 - 669$ keV for the 2614 keV gate based on ^{208}Tl-decay photons (thorium series); $1024 - 1324$ keV for the 609 keV gate based on ^{214}Bi-decay photons (uranium series).

[c] Based on an activity of 55.4 ± 0.1 Bq for the thorium reference sample (Section 3.1).

[d] Based on an activity of 341 ± 2 Bq for the uranium reference sample (Section 3.1).

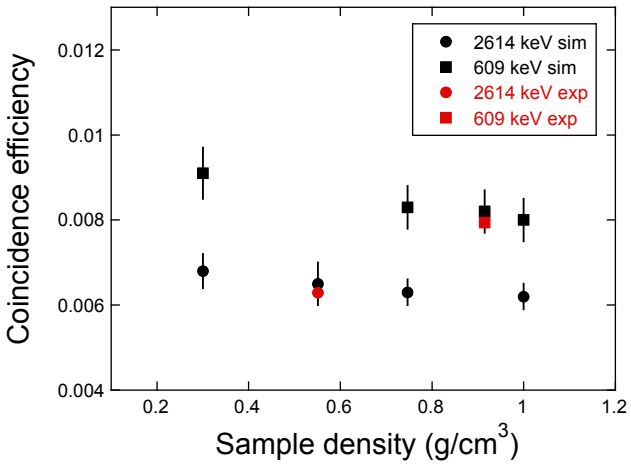

Figure 5: (Colour online) Coincidence efficiencies for the 2614 keV (circles) and 609 keV (squares) gates versus sample density. The black and red data points correspond to simulated and measured efficiencies, respectively. The efficiency is decreasing with increasing density because of self-absorption of γ-rays in the sample. The displayed density values, from left to right, correspond to: potting mix (0.300 g/cm^3), thorium reference (0.551 g/cm^3), Brazil nuts (0.747 g/cm^3), uranium reference (0.917 g/cm^3), and magazine paper (1.01 g/cm^3). Notice that the uncertainties of the experimental values are smaller than the symbol size.

Table 2: Measured singles and coincidence background count rates, in units of counts per minute (cpm), using distilled water inside the sample holder; A_{min} is the minimum detectable activity (in mBq).

Energy region (keV)	Decay	Singles (cpm)	Coincidence (cpm)	A_{min} (mBq)[a]
444 − 669	^{208}Tl	148	0.10[b]	41
1024 − 1324	^{214}Bi	77	0.13[c]	36

[a] Applicable for a counting time of 3 d; A_{min} approximately scales with the inverse square root of the counting period.

[b] The coincidence gate is based on an energy of 2614 keV (see top panel in Figure 2).

[c] The coincidence gate is based on an energy of 609 keV (see bottom panel in Figure 2.

The top panel of Figure 6 reveals a small peak in the region of interest. It is caused by the 2614 keV gate crossing the 511 keV annihilation band. The latter most likely originates from pair production and cosmic-ray muon interactions. Two peaks are visible in the bottom panel below the energy region of interest. The 511-keV peak has the same origin as in the top panel. Photons at 1461 keV from ^{40}K decay can Compton scatter and deposit energy in both detectors. Such coincidence events show up mainly in the two-dimensional histogram as a diagonal band with a total energy of 1461 keV. When this diagonal band crosses the coincidence gate at 609 keV, it produces a peak at 852 keV (= 1461 keV minus 609 keV).

From the number of background counts, we estimated the minimum detectable activity, A_{min}. The A_{min} values were calculated using the expression $A_{min} = N_{min}/(\eta_{coin} t_m)$, with N_{min} the minimum number of signal (i.e., total minus background) counts in the region of interest, η_{coin} the coincidence detection efficiency listed in Table 1, and t_m the duration of the background measurement. The quantity N_{min} was estimated from the total number of observed background counts in a given coincidence gate using Bayesian inference [12]. The observed total and background counts were modeled according to Poissonian distributions. Several different non-informative priors were tested (uniform, Gaussians with large widths, etc.) and gave similar results. The resulting minimum detectable activities, corresponding to 97.5 percentiles of the posterior density, are listed in the last column of Table 2.

Our minimum detectable activity of ≈ 40 mBq agrees approximately with the result of Ref. [11], who quotes values of 22 mBq and 74 mBq for food and soil, respectively, for a counting period of 1000 min. The minimum detectable activity scales approximately with the inverse square root of the counting period.

4. Environmental Sample Measurements and Results

Figures 7 and 8 show our measured coincidence spectra, gated on the 2614 keV (from ^{208}Tl decay) and 609 keV (from ^{214}Bi decay) γ-rays, respectively, as red histograms. The coincidence background, obtained

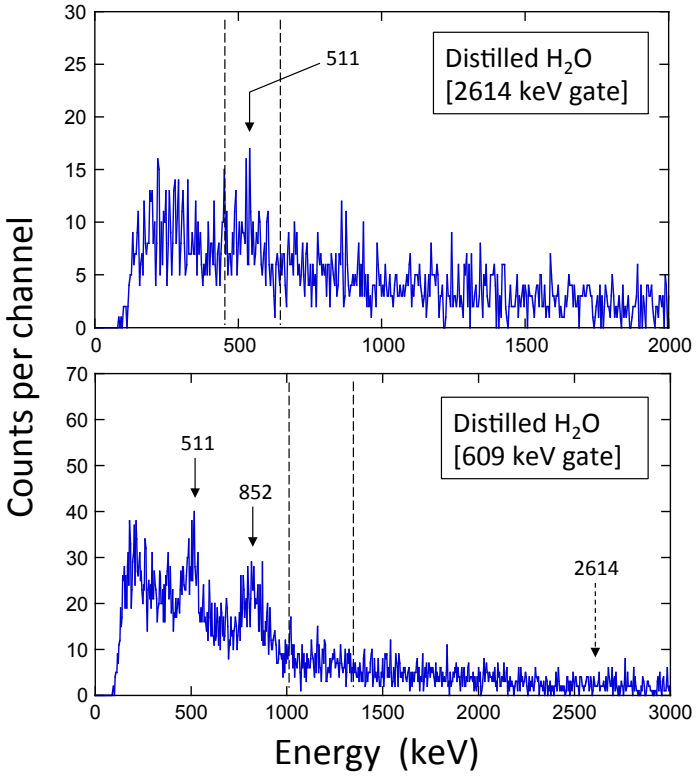

Figure 6: (Colour online) Measured background of events located inside the red coincidence gates shown in Figure 2, obtained using distilled water in the sample holder. Regions of interest are indicated by vertical dashed lines. The measurement time was 71.6 h. (Top) The coincidence gate is based on 2614 keV from ^{208}Tl decay. The small peak in the region of interest (444 − 669 keV) is caused by the gate crossing the 511 keV annihilation band. (Bottom) The coincidence gate is based on 609 keV from ^{214}Bi decay. Two peaks appear below the region of interest (1024 − 1324 keV). The broad peak at 852 keV (1461 keV minus 609 keV) is caused by 1461 keV background photons from ^{40}K Compton scattering between the two detectors. The peak at 511 keV is caused by the gate crossing the 511 keV annihilation band.

using distilled water, is shown as the blue histogram. Since we waited one month between the preparation of the samples and the measurement, the short-lived ^{208}Tl is in secular equilibrium with ^{228}Th (1.9 y half-life), and perhaps with another parent isotope further up the decay chain depending on environmental chemistry, and the short-lived ^{214}Bi is in secular equilibrium with ^{226}Ra (1600 y half-life). Our measured ^{228}Th and ^{226}Ra activities are listed in Table 3 and compared to values from the literature.

4.1. Brazil Nuts

The Brazil nut tree (*Bertholletia excelsa*), which is native to the Amazon region, has a high capacity for barium uptake from the soil. Barium and radium have similar chemical properties and, therefore, the latter radioisotope accumulates in the nuts. As a result, the radioactivity in Brazil nuts is higher by a few orders of magnitude compared to other foods [16].

The 2614-keV gated spectrum (top panel in Figure 7) displays the coincident 511-keV and 583-keV peaks from ^{208}Tl decay with the expected intensity ratio. From the number of counts above background and the coincidence efficiency listed in Table 1, we find an activity of 21.3 ± 1.7 mBq/g for ^{228}Th (see Table 3). Unlike radium, thorium shows very little mobility in the environment; when the roots of the Brazil nut tree take up radium and barium, most of the thorium should remain in the soil. Therefore, the measured ^{228}Th activity in Brazil nuts most likely derives from the plant uptake of ^{228}Ra ($T_{1/2} = 5.8$ y). However, since we have not measured the ^{228}Ra activity, we may not claim secular equilibrium between ^{228}Th and ^{228}Ra. Our result for ^{228}Th is in the upper range of activities reported by Ref. [17], but is about twice as high as the values listed in Ref. [15]. The latter work used a perforated sample holder, and the reported activities could not be corrected for ^{220}Rn emanation losses. Notice that in both previous works the activities were derived from decays of ^{208}Tl and ^{212}Pb, and were attributed to ^{224}Ra. However, because of the short half-life of ^{224}Ra ($T_{1/2} = 3.6$ d), ^{208}Tl and ^{212}Pb must have been in secular equilibrium with a parent isotope further up the decay chain, most likely ^{228}Th (and pehaps ^{228}Ra).

The 609-keV gated spectrum (top panel of Figure 8) displays the coincident 1120-keV and 1238-keV peaks from ^{214}Bi decay with the expected intensity ratio. However, notice the peak at 2614 keV, which is absent in the distilled water spectrum (blue histogram). It results from ^{208}Tl, i.e., (583, 2614) coincidences, in the Brazil nut sample. Consequently, we expect that Compton scattered photons from such events will give rise to an additional background in the region of interest (indicated by the dashed vertical lines). This background was estimated using the Geant4 toolkit (Section 3.3) by repeating the ^{208}Tl decay simulations for the 609 keV gate. We find for the ratio of counts in the 2614 keV peak and the intensity of Compton-scattered events in the region of interest a value of ≈ 4.5. Subtracting the measured background (blue histogram) and the simulated contribution from Compton-scattered ^{208}Tl decay photons from the measured Brazil nut spectrum (red histogram), we find a ^{226}Ra activity of 33.1 ± 2.4 mBq/g (see Table 3). Our result agrees with that of Ref. [18], and is in marginal agreement with the values listed in Ref. [15]. Our result is

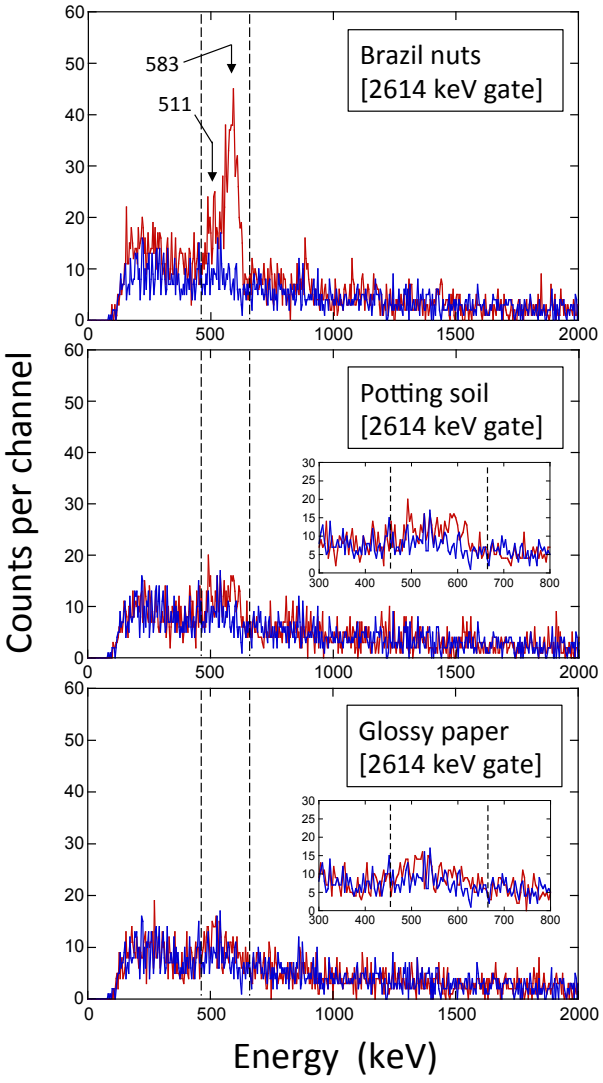

Figure 7: (Colour online) Concidence spectra of (top) Brazil nuts, (middle) potting mix, and (bottom) magazine paper are show as red histograms. The blue histogram was obtained with distilled water and is the same as that shown in Figure 6 (top). The coincidence gate was based on 2614 keV (see top of Figure 2) and the region of interest is marked by the two vertical dashed lines. Some of the important peaks are marked with energies in units of keV; see top panel of Figure 3. The insets show a magnified view of the region of interest. No significant excess in counts above background is observed in the bottom panel. The measurement time was 3.0 days.

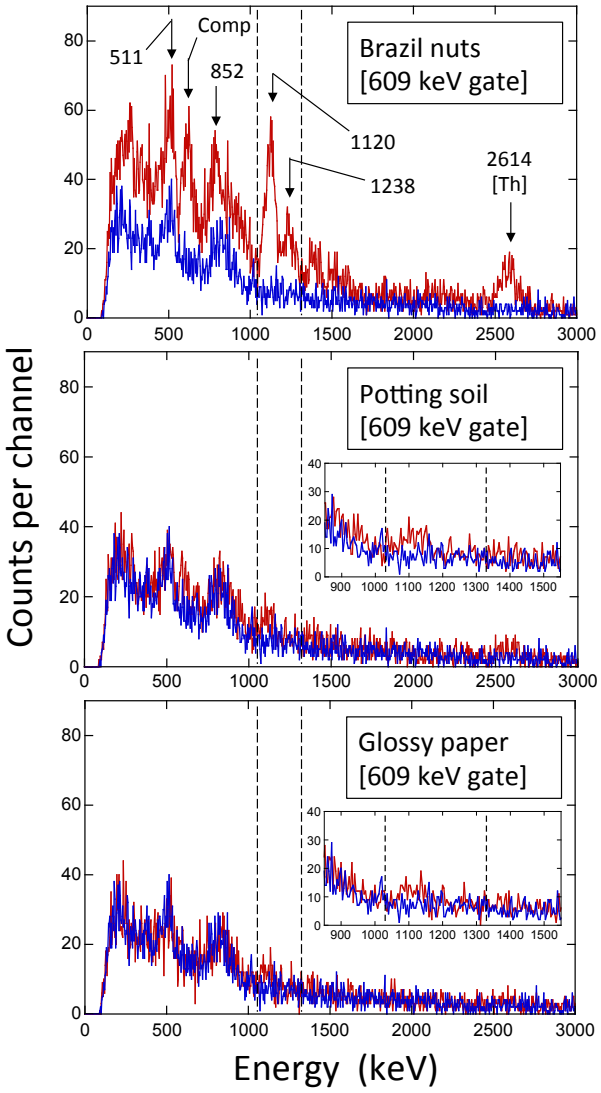

Figure 8: (Colour online) Concidence spectra of (top) Brazil nuts, (middle) potting mix, and (bottom) magazine paper are show as red histograms. The blue histogram was obtained with distilled water and is the same as that shown in Figure 6 (bottom). The coincidence gate was based on 609 keV (see bottom of Figure 2) and the region of interest is marked by the two vertical dashed lines. Some of the important peaks are marked with energies in units of keV; see bottom panel of Figure 3. The insets show a magnified view of the region of interest. Significant excesses in counts above background are observed for all samples. The measurement time was 3.0 days.

Table 3: Measured activities (in units of mBq/g dry weight) in environmental samples.

Sample	Brazil nuts	Potting mix	Magazine paper
Weight (g)	17.980	7.226	24.231
present (^{228}Th)[a]	21.3 ± 1.7	12.4 ± 2.6	≤ 1.8
previous	$7 - 14$[c,e]	$4 - 130$[g,h]	$12 - 30$[i,j]
	$11 - 22$[d,e]		
present (^{226}Ra)[b]	33.1 ± 2.4	13.2 ± 2.3	2.5 ± 0.7
previous (^{226}Ra)	$17 - 31$[c]	$8 - 160$[g]	$3.5 - 11$[i]
	$79 - 135$[d]		
	$26 - 65$[f]		

[a] Present results derived from the measured decay of ^{208}Tl. The coincidence gate is based on an energy of 2614 keV in one detector, and a region of $444 - 669$ keV in the other detector.

[b] Present results derived from the measured decay of ^{214}Bi. The coincidence gate is based on an energy of 609 keV in one detector, and a region of $1024 - 1324$ keV in the other detector.

[c] From Ref. [15]. Four different values were determined for different regions in South America.

[d] From Ref. [17]; mean values for different sizes of Brazil nuts.

[e] The quoted activities, derived from decays of ^{208}Tl and ^{212}Pb, were attributed to ^{224}Ra ($T_{1/2} = 3.6$ d).

[f] From Ref. [18]; mean values for Brazil nuts sold between 2010 and 2013.

[g] From Ref. [19]; the quoted literature values are for soils in the United States, not for potting mix.

[h] The activity is reported for ^{232}Th ($T_{1/2} = 14.0$ Gy).

[i] From Ref. [20]; the quoted literature values are for journals published in the United States. Smaller activities have been reported for journals from some other countries.

[j] The quoted activities, derived from decay of ^{208}Tl, were attributed to ^{232}Th ($T_{1/2} = 14.0$ Gy).

on average lower by a factor of three compared to the values published in Ref. [17].

4.2. Potting Mix

Commercial potting mix, also called potting soil, consists of sand, perlite, bark, compost, and other ingredients. Despite its name, it contains little soil. The manufacturer guaranteed chemical analysis stated 0.113% ammoniacal nitrogen, 0.097% nitrate nitrogen, 0.11% P_2O_5, and 0.16% K_2O.

The middle panel in Figure 7 shows the 2614-keV gated spectrum. The sample and background spectra are matched at the low and high energy end of the region of interest (vertical dashed lines). An excess of counts in the sample spectrum (red) is observed at the location of the 511-keV and 583-keV peaks from ^{208}Tl decay. Based on the number of counts above background and the coincidence efficiency listed in Table 1, we find a ^{228}Th activity of 12.4 ± 2.6 mBq/g (see Table 3).

The 609-keV gated spectrum (middle panel of Figure 8) reveals an excess of counts in the sample spectrum (red) at the location of the 1120-keV peak from ^{214}Bi decay. Subtraction of the measured background (blue histogram) and the simulated contribution from Compton-scattered ^{208}Tl decay photons from the measured potting mix spectrum (red histogram) yields a ^{226}Ra activity of 13.2 ± 2.3 mBq/g (see Table 3).

We could not find any previously published ^{228}Th or ^{226}Ra activities for potting mix. However, our results are in the range of values reported for soils in the United States ($4 - 130$ mBq/g for ^{232}Th, $8 - 160$ mBq/g for ^{226}Ra; see Ref. [19]). Our results do not support claims of an increased radioactivity in potting mix on some websites.

4.3. Magazine Paper

Among the many ingredients used in the papermaking process are nonfibrous, insoluble mineral materials called fillers. They impart specific properties to the paper, such as whiteness, improved ink receptivity, and surface smoothness. Commonly used fillers are clay, calcium carbonate, and TiO_2. The clay used in the process of fabricating glossy paper is a potential source of thorium and uranium.

The 2614-keV gated spectrum is shown in the bottom panel of Figure 7. The sample and background spectra show a similar number of counts in the region of interest (vertical dashed lines) and, therefore, only an upper limit could be obtained for the ^{228}Th activity in the paper sample. Using a Bayesian model (Section 3.4), we find a value of ≤ 1.8 mBq/g using the 97.5 percentile of the posterior density. The radioactivity in fine papers, used for journals published in the United States, has been studied in Taylor & Singh [20]. By measuring the decay of ^{208}Tl, they find an activity range of $12 - 30$ mBq/g. They assume secular equilibrium between ^{208}Tl and ^{232}Th, although there is little evidence to support this assumption.

The 609-keV gated spectrum (bottom panel of Figure 8) shows an excess of counts in the sample spectrum (red) at the location of the 1120-keV peak from ^{214}Bi decay. Subtraction of the measured background (blue histogram) from the measured magazine paper spectrum (red histogram) yields a ^{226}Ra activity of

2.5 ± 0.7 mBq/g (see Table 3). Our result is near the lower end of the previously [20] reported ^{226}Ra activities ($3.5 - 11$ mBq/g).

5. Summary and Conclusions

We discussed the performance of a $\gamma\gamma$-coincidence spectrometer for measuring thorium and uranium daughters in environmental samples. The coincidence efficiencies for γ-ray cascades from ^{208}Tl and ^{214}Bi decay are small ($< 1\%$), but at the same time the coincidence room background is lower by three orders of magnitude compared to the singles count rate. We described the most favorable coincidence gating schemes, detection efficiencies, background count rates, and minimum detectable activities. Our spectrometer has been fully simulated using Geant4, and the simulations are used to correct detection efficiencies for self-absorption effects that depend on the type of sample being measured.

We employed the device to estimate thorium and uranium daughter activities in three different samples: Brazil nuts, potting mix, and magazine paper. Our uranium and thorium activities for Brazil nuts agree with some, but not all, previous measurements. Neither thorium nor uranium activities have previously been reported for commercial potting mix. Our measured values are in the range of activities reported for various soils in the United States. For magazine paper, our measured activities are lower than previously determined results.

The sensitivity of the spectrometer could be further increased by replacing the photomultiplier tubes of the NaI(Tl) detectors, and by using an active shield (i.e., cosmic-ray muon veto).

Acknowledgement

We would like to thank Richard Longland, John Wilkerson, and John Kelley for providing helpful comments. This work was supported in part by the U.S. Department of Energy under Contract No. DE-FG02-97ER41041.

References

[1] Roedel, W., 1970. On low-level-counting of positron emitters. Nucl. Instr. Meth. 83, 88-92.

[2] Cooper, J. A. and Perkins, R. W., 1971. An anticoincidence-shielded dual Ge(Li) gamma-ray spectrometer for low-level environmental radionuclide analysis and gamma-gamma coincidence studies. Nucl. Instr. Meth. 94, 29-38.

[3] Povinec, P., 1981. Dual parameter gamma-ray spectrometer for low-level counting. Isotopenpraxis 18, 92-95.

[4] Grismore, R., et al., 1998. A very-low-level gamma-ray analysis system for modest laboratories. Nucl. Instr. Meth. A 402, 164-170.

[5] Zhang, W., Yi, J., Mekarski, P., Hoffman, I., Ungar, K., and Leppänen, A.-P., 2011, A system for low-level the cosmogenic 22Na radionuclide measurement by gamma–gamma coincidence method using BGO detectors. J. Radioanaly. Nucl. Chem. 287, 551-555.

[6] Burnett, J.L., and Davies, A.V., 2011. Investigating the time resolution of a compact multidimensional gamma-spectrometer. J. Radioanaly. Nucl. Chem. 288, 699-703.

[7] Britton, R. Burnett, J., Davies, A., and Regan, P.H., 2012, Preliminary simulations of NaI(Tl) detectors, and coincidence analysis using event stamping. J. Radioanaly. Nucl. Chem. 295, 573-577.

[8] Zhang, W., Ungar, K., Stukel, M., and Mekarski, P., 2014. A gamma-gamma coincidence/anticoincidence spectrometer for low-level cosmogenic ^{22}Na/^{7}Be activity ratio measurement. J. Environ. Radioact. 130, 1-6.

[9] Tillett, A., Dermigny, J., Emamian, M., Tonin, Y., Bucay, I., Smith, R.L., Darken, M., Dearing, C., Orbon, M., and Iliadis, C., 2017. A low-background $\gamma\gamma$-coincidence spectrometer for radioisotope studies. Nucl. Instr. Meth. A 871, 66-71.

[10] Swartz, K.B., Visser, D.W., and Baris, J.M., 2001. A Java-based data acquisition system for nuclear physics. Nucl. Instr. Meth. A 463, 354-360.

[11] Sanderson, C.G., 1969. Determination of ^{226}Ra and ^{228}Th in food, soil, and biological ash by multidimensional coincident gamma-ray spectrometry. Health Phys. 16, 747.

[12] Andreon, S., and Weaver, B., 2015. Bayesian Methods for the Physical Sciences (Springer International Publishing).

[13] Agostinelli, S., et al. (*Geant4 Collaboration*), 2003. Geant4 - a simulation toolkit. Nucl. Instr. Meth. A 506, 250-303; version `Geant4.8.1-p1`.

[14] Paradis, H., de Vismes Ott, A., Luo, M., Cagnat, X., Piquemal, F., and Gurriaran, R. 2016. Low level measurement of ^{60}Co by gamma ray spectrometry using $\gamma - \gamma$ coincidence. Appl. Rad. Isotop. 109, 487-492.

[15] Parekh, P.P., Khan, A.R., Torres, M.A., and Kitto, M.E., 2008. Concentrations of selenium, barium, and radium in Brazil nuts. J. Food Comp. Anal. 21, 332-335.

[16] Turner, R.C., Radley, J.M., and Mayneord, V.W., 1958. The Naturally Occurring Alpha-Ray Activity of Foods. Health Phys. 1, 268-275.

[17] Martins, M., Pacheco, A.M., Lucas, A.C., Andrello, A.C., Appoloni, C.R., and Xavier, J.M., 2012. Brazil nuts: determination of natural elements and aflatoxin. Acta Amazonica 42, 157-164.

[18] Armelin, M.J.A., Maihara, V.A., Cozzolino, S.M.F., Silva, P.S.C., and Saiki, M., 2016. Activity levels of gamma-emitters in Brazil nuts. Brazilian J. Rad. Sciences 04-01, 1-9.

[19] United Nations Scientific Committee on the Effects of Atomic Radiation (UNSCEAR), 2000. Sources and Effects of Ionizing Radiation (Report to the General Assembly), Vol. 1, p. 155. United Nations, New York.

[20] Taylor, H.W., and Singh, B., 1993. Radioactivity in fine papers. J. Environ. Radioactivity 21, 177-187